Am J Physiol Heart Circ Physiol 303: H1096–H1106, 2012.
First published August 24, 2012; doi:10.1152/ajpheart.00438.2012.

Autoregulation and mechanotransduction control the arteriolar response to small changes in hematocrit

Krishna Sriram,[1] Beatriz Y. Salazar Vázquez,[2,3] Amy G. Tsai,[2] Pedro Cabrales,[2] Marcos Intaglietta,[2] and Daniel M. Tartakovsky[1]

[1]*Department of Mechanical and Aerospace Engineering, University of California-San Diego, La Jolla, California;* [2]*Department of Bioengineering, University of California-San Diego, La Jolla, California; and* [3]*Department of Experimental Medicine, Faculty of Medicine, Universidad Nacional Autónoma de México, Hospital General de México, México City, Mexico*

Submitted 6 June 2012; accepted in final form 20 August 2012

Sriram K, Salazar Vázquez BY, Tsai AG, Cabrales P, Intaglietta M, Tartakovsky DM. Autoregulation and mechanotransduction control the arteriolar response to small changes in hematocrit. *Am J Physiol Heart Circ Physiol* 303: H1096–H1106, 2012. First published August 24, 2012; doi:10.1152/ajpheart.00438.2012.—Here, we present an analytic model of arteriolar mechanics that accounts for key autoregulation mechanisms, including the myogenic response and the vasodilatory effects of nitric oxide (NO) in the vasculature. It couples the fluid mechanics of blood flow in arterioles with solid mechanics of the vessel wall and includes the effects of wall shear stress- and stretch-induced endothelial NO production. The model can be used to describe the regulation of blood flow and NO transport under small changes in hematocrit and to analyze the regulatory response of arterioles to small changes in hematocrit. Our analysis revealed that the experimentally observed paradoxical increase in cardiac output with small increases in hematocrit results from the combination of increased NO production and the effects of a strong myogenic response modulated by elevated levels of WSS. Our findings support the hypothesis that vascular resistance varies inversely with blood viscosity for small changes in hematocrit in a healthy circulation that responds to shear stress stimuli. They also suggest beneficial effects independent of changes in O_2 carrying capacity associated with the postsurgical transfusion of one or two units of blood.

indexable words: autoregulation; arterioles; mechanotransduction; blood rheology; hematocrit change; cardiac output; blood transfusion

THE EXISTENCE of a direct relationship between blood viscosity [and hematocrit (Hct)] and blood pressure is a widely held assumption also supported by epidemiological studies (13, 28). However, this finding may be more applicable to the older population, where endothelial dysfunction mitigates the vasodilatory response of increased vessel wall shear stress (WSS), or when the induced hemoconcentration exceeds the variability of Hct found in the normal population (40). The influence of changes in Hct on blood pressure and cardiac output (CO) within the range of changes found in the normal population has been studied experimentally (30, 43) and shows a counterintuitive behavior, whereby small Hct increases are associated with decreased blood pressure and increased CO. An explanation for this behavior is that increased Hct and fluid viscosity increase WSS (42) in arterioles, thus increasing nitric oxide (NO) production by the endothelium (32, 33). This increased NO production promotes vasodilation (2), causing blood pressure to decrease and CO to increase (43). The existence of this mechanism was confirmed by experiments in which the administration of *N*-nitro-l-arginine methyl ester (L-NAME) blocked NO production by the endothelium, negating this effect.

The administration of L-NAME causes general vasoconstriction of the vasculature, which may overcome additional vasodilator mechanisms induced by the increase in Hct and blood viscosity (43). Furthermore, the effects on blood pressure, CO, and peripheral vascular resistance are comparatively large relative to the magnitude of the WSS stimulus, suggesting the existence of additional non-NO-dependent mechanisms.

The behavior of the circulation (and corresponding regulation) is influenced by coupled physical and biochemical phenomena, including the myogenic response, stimulation by the sympathetic nervous system, effects of shear stress, etc. (12, 20). In addition, blood O_2 carrying capacity increases with Hct, thereby reducing the blood flow required to maintain a constant level of O_2 delivery (5).

Several previous studies (3, 7, 23, 46) have focused on the development of mathematical models of blood flow regulation by the vasculature. These models describe the mechanics of the vascular wall exposed to internal pressure and the corresponding effects on vessel tone. They also provide mathematical descriptions of the myogenic response and WSS-induced effects and of the coupled behavior of blood flow and the mechanics of the vessel wall. These studies modeled the behavior of vessel walls by relying on Laplace's law, which is rigorously valid for thin elastic cylinders (46) and remains accurate as long as the ratio of a vessel's wall thickness to its diameter exceeds 10 (ideally 20 or more) (55). While this condition is applicable to arteries, it breaks down for arterioles, where this ratio can be as small as 2 or even less (38). Finally, these models described the effects of WSS on vascular tone using simple constitutive laws relating WSS with vessel wall tension, without accounting for the variation of NO bioavailability in the vascular wall due to WSS changes.

Motivated by the experimentally observed changes in blood pressure with Hct, we modeled the dependence of blood flow (and CO) on systemic Hct by treating arterioles as thick, elastic cylinders (54, 61) and coupling hemodynamics and vessel mechanics. The model allowed us to investigate the effects of this coupling on autoregulation and to describe changes in the wall thickness with changing intraluminal pressure. The latter is a crucial factor for calculating NO transport in the vasculature. We evaluated the concentration profiles of NO in the vessel wall (51) to account for the vasodilation due to WSS-induced NO production.

Address for reprint requests and other correspondence: M. Intaglietta, Dept. of Bioengineering, Univ. of California-San Diego, 9500 Gilman Dr., La Jolla, CA 92093-0412 (e-mail: mintagli@ucsd.edu).

Experimental studies to describe the mechanical properties of arteries and arterioles typically quantify elastic moduli (15) or develop length-tension curves for individual blood vessels. The observed mechanical behavior is reported as a constitutive law (23, 46) comprising active and passive (elastic/viscoelastic) components. Our model accounts for both active and passive stresses. Passive stress is determined by intraluminal pressure; active stress (the myogenic response) is a function of tension in the vessel wall (6, 20, 46). Here, we account for the relationship between pressure and radius of arterioles for small changes in pressure and then describe the effect of varying Hct on flow rate through the blood vessel (and hence CO).

METHODS

Simulation Domain

We considered an arteriole with the vascular wall tethered to adjoining connective tissue, which prevents axial motion of the blood vessel (37). The arteriole is modeled as a thick cylinder composed of an isotropic, elastic material (6, 54). We described both the passive radial deformation of the vessel under internal pressure (i.e., the passive response of the arteriole to intraluminal blood pressure) and the myogenic response of the vessel walls to this pressure, which acts to reduce vessel diameter as intraluminal pressure increases (21). Blood flow within the arteriole is assumed to be a two-layer flow, consisting of a red blood cell (RBC)-rich core and a plasma layer devoid of RBCs (47, 51, 61). The arteriole was assumed to be surrounded by easily deformable tissue, which exerts negligible compressive stress on the vessel walls.

Blood Flow

We considered steady one-dimensional flow in a cylinder (arteriole) of inner radius R. Blood was modeled as a two-layer fluid, consisting of a RBC-rich core and a plasma layer (Fig. 1). Following Refs. 26 and 51, we assumed the following linear relationship between the plasma layer thickness (δ) and systemic Hct (H_d):

$$\delta = a_3 H_d + a_4 \quad (1)$$

where a_3 and a_4 are fitting parameters. H_d and core Hct (H_c) are related as follows (51):

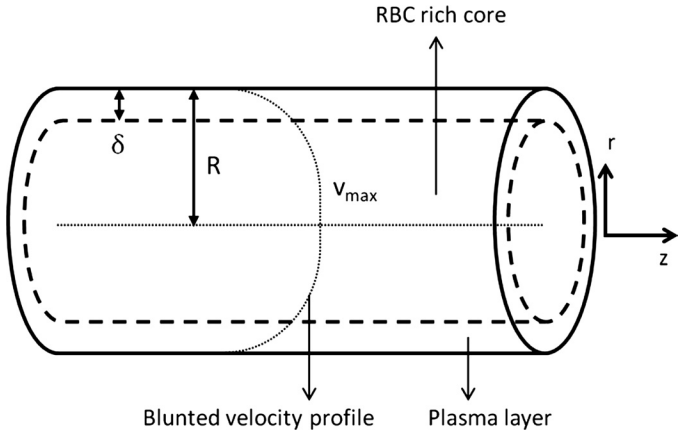

Fig. 1. Two-phase flow of blood in a cross section of an arteriole with a cell-free layer and red blood cell (RBC)-rich core, resulting in a blunted velocity profile. δ, Plasma layer thickness; R, inner radius; v_{max}, maximum velocity; r, radial distance from the centerline; z, axial coordinate.

$$H_d = 2H_c\lambda^2\left(1-\lambda^2+\lambda^2\frac{\mu_p}{2\mu_c}\right)\left(1-\lambda^2+\lambda^2\frac{\mu_p}{\mu_c}\right)^{-1}, \quad \text{where } \lambda = 1-\frac{a_3H_d+a_4}{R} \quad (2)$$

where λ is the plasma layer thickness and μ_c and μ_p are the viscosities of core blood and plasma, respectively. We made use of the following experimentally obtained linear relationship for blood viscosity in the RBC-rich core as a function of H_c (30, 51): $\mu_c = a_1H_c + a_2$, where the fitting parameters a_1 and a_2 were set to $a_1 = 0.1678$ and $a_2 = -4.348$ cP. The positive root of *Eq. 2* yielded a relationship between H_d and H_c, which was approximately linear over a physiologically relevant range of H_d (51).

According to the two-phase model of blood flow in a vessel, blood flow rate (Q) and pressure gradient (J) are related as follows (47, 51):

$$Q = \frac{\pi JR^4}{8\mu_p}\left(\frac{\mu_p}{\mu_c}\lambda^4 + 1 - \lambda^4\right) \quad (3)$$

The corresponding WSS (τ) is given as follows:

$$\tau = JR/2 \quad (4)$$

For constant Q, τ has been shown to be linearly related to Hct ($R^2 = 0.997$) in a previous study (see Fig. 3 in Ref. 51).

Vessel Mechanics

Following Refs. 6, 7, and 46, we assumed the vessel to be elastic and to exhibit both active and passive responses to blood flow. The elastic model treats the blood vessel as a tethered cylinder, i.e., neglects strain in the axial direction (44), and postulates a linear relationship between radial strain (u) and the radial (σ_r) and circumferential (σ_θ) components of the stress tensor on the vessel walls (54, 61):

$$u(r) = \frac{r}{E}\left[\sigma_\theta(1-\nu^2) - \nu\sigma_r(1+\nu)\right] \quad (5)$$

where $r \in [R, R_o]$ is the radial distance from the vessel's centreline, which varies between R and the outer radius (R_o) of the vessel's walls; E is the elastic modulus of the blood vessel; and ν is the Poisson ratio. We assumed that E is constant (6) and that the vessel wall is incompressible. The latter assumption is justified by the high water content of the tissue (54, 61) and allowed us to set $\nu = 0.5$ in all simulations reported below.

The vessel's active and passive responses to blood flow were modeled by representing $\sigma_r = \sigma_{rp} + \sigma_{ra}$ and $\sigma_\theta = \sigma_{\theta p} + \sigma_{\theta a}$ as the sums of their respective passive (σ_{rp} and $\sigma_{\theta p}$) and active (σ_{ra} and $\sigma_{\theta a}$) components. The passive response represents the stress induced by blood flow on the vessel's wall. The corresponding components of the mechanical stress were derived from Lame's equations (55) as follows:

$$\sigma_{rp} = \frac{R^2P}{R_o^2-R^2}\left(1-\frac{R_o^2}{r^2}\right) \text{ and } \sigma_{\theta p} = \frac{R^2P}{R_o^2-R^2}\left(1+\frac{R_o^2}{r^2}\right) \quad (6)$$

where P is intraluminal blood pressure. The active (myogenic) response accounts for the Bayliss effect, which acts to reduce the vessel's radius in response to increasing pressure (11, 20). It is assumed to be linearly proportional to the tension at the surface of the vessel wall, $PR/2$, such that (6, 20):

$$\sigma_{ra} = \frac{R^2}{R_o^2-R^2}\left(1-\frac{R_o^2}{r^2}\right)\frac{-\varphi CPR}{R_{eq}} \text{ and } \sigma_{\theta a} = \frac{R^2}{R_o^2-R^2}\left(1+\frac{R_o^2}{r^2}\right)\frac{-\varphi CPR}{R_{eq}} \quad (7)$$

where R_{eq} is the vessel radius at equilibrium at baseline pressure, C is a fitting parameter, and

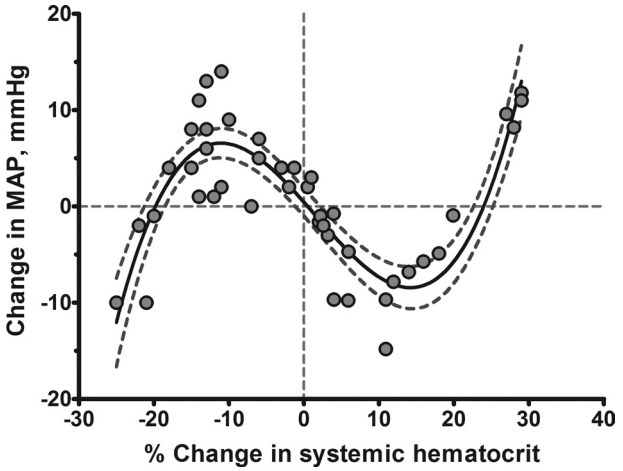

Fig. 2. Experimental measurement of variations of mean arterial pressure (MAP) with small changes in hematocrit (Hct) from baseline (31, 43). The same results were obtained in CD-1 mice but not in endothelial nitric oxide (NO) synthase knockout mice (30). Round symbols indicate data for a single animal, solid line is the best 3rd order polynomial fit of the data, and the dotted lines indicate 95% confidence interval for the curve fit.

$$\varphi = \tanh\left(\frac{\alpha}{\tau}\right) \tag{8}$$

φ represents the modulation of the myogenic response by the WSS [which was normalized with a fitting parameter (α)] (23). *Equations 7* and *8* account for experimental observations (22) showing that large values of WSS reduce the strength of the myogenic response.

Model Closure

To close the system of *Eqs. 1–8*, we used experimental observations (18) and the modeling assumption in Ref. 7, according to which changes in J in the arteriole are directly proportional to changes in P, as follows:

$$\Delta J \propto \Delta P \tag{9}$$

This assumption is also justified by the role of autoregulation in ensuring a relatively constant hydrostatic capillary pressure (12, 20), which implies that larger mean arterial pressures (MAPs) (and hence larger P) necessitate larger blood pressure gradients in arterioles.

Finally, we allowed for variations of P with Hct. We adapted a relationship that mirrors the experimentally observed (7, 31, 43) response of MAP (and hence P) to small but acute changes in Hct during both hemoconcentration and hemodilution, as shown in Fig. 2. The change in MAP (and, consequently, in P) from baseline with H_d is given as follows:

$$\Delta P = 0.01996H_d^3 - 2.7048H_d^2 + 120.32H_d - 1758.8 \tag{10}$$

NO Production

Shear-induced NO production. Experimental data (32, 33) have suggested that, for physiological levels of shear stress, endothelial NO production varies approximately linearly with τ. We modeled this phenomenon by assuming that NO production follows Michaelis-Menten kinetics (8), so that the corresponding reaction rate (R_e) is given as follows:

$$R_e = \frac{R_{NOm}Po_2}{Po_2 + K_m} \tag{11}$$

Here, the maximum rate of NO production (R_{NOm}) increases linearly with τ. Po_2 is the partial pressure of O_2, and the value of the Michaelis-Menten constant (K_m) is shown in Table 1.

Stretch-induced NO production. The data reported in Refs. 3, 24, and 59 show that not only τ but also mechanical stretch of the endothelium affects NO production. Furthermore, experimental evidence (24) has suggested that circumferential stretch increases NO production even when WSS is kept constant. In the absence of detailed quantitative studies of this phenomenon, we assumed that R_{NOm} is proportional to small variations of the vessel radius.

Combining these two mechanisms of NO production, we postulated that R_{NOm} responds to mechanical forces according to the following:

$$R_{NOm} = R_{NOmax}\tau\left(1 + \frac{\Delta R}{R_{eq}}\right)^L \tag{12}$$

where L is a fitting parameter and the constant maximum NO production rate in the endothelium (R_{NOmax}) is shown in Table 1. The simulation results presented below suggest that the stretch-induced mechanism is crucial to the vasodilatory activity of NO.

NO Transport

We relied on the Krogh tissue model (Fig. 3) to describe the various layers comprising the vessel tissue and lumen and on a system of reaction-diffusion equations (26, 51) to model the radial (one-dimensional) transport of NO across these layers.

RBC-rich core ($0 \le r \le R - \delta$). Po_2 was assumed to be constant (26), and NO concentration (C_{NO}) satisfied the following steady-state reaction-diffusion equation:

Table 1. *Model parameters used*

Parameter	Symbol	Value	Reference(s)
Solubility of O_2	γ	1.34 μM/Torr	26, 51
Diffusivity of O_2 in "fluid" layers	D_{O_2}	2,800 $\mu m^2/s$	26, 51
Diffusivity of NO in "fluid" layers	D_{NO}	3,300 $\mu m^2/s$	26, 51
Diffusivity of O_2 in "solid" layers	D_{O_2}	2,800 or 1,400 $\mu m^2/s$	17
Diffusivity of NO in "solid" layers	D_{NO}	3,300 or 1,650 $\mu m^2/s$	17, 51
Maximum O_2 consumption rate in tissue	$R_{O_2,max}$	20 μM/s	26, 51
Maximum NO production rate in endothelium	$R_{NO,max}$	150 μM/s	26, 51
Scavenging rate of NO in blood at 45% Hct	λ_b	382.5 s^{-1}	26, 51
Rate of consumption of NO in tissue	λ_t	1 s^{-1}	26, 51
Michaelis-Menten constant for NO in endothelium	K_m	4.7	8
Ratio of diffusion coefficients of species in the solid phase to the liquid phase	D_r	1 or 1/2	17
Unstressed arteriole inner diameter (i.e., fluid domain)	R	20 μm	
Unstressed endothelial thickness		1 μm	
Unstressed vascular wall		10 μm	
Elastic modulus of the vessel wall	E	10000 Nm^{-2}	50
Constant in *Eq. 7*	C	8	

NO, nitric oxide; Hct, hematocrit.

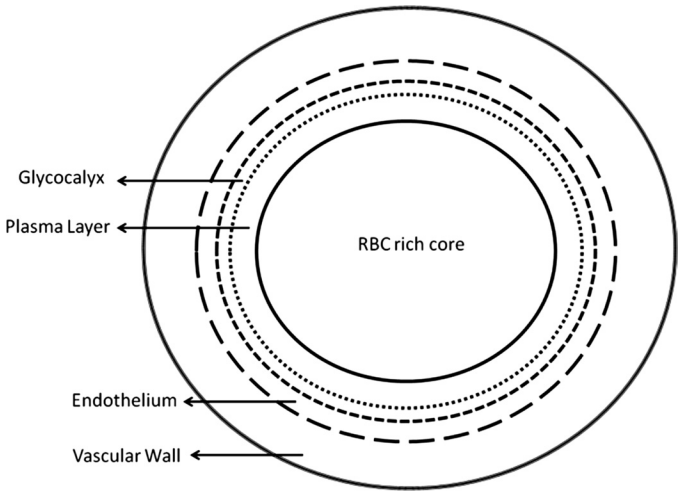

Fig. 3. Cross section of an arteriole. The version of the Krogh tissue cylinder model used in our analysis consisted of a RBC-rich core, a RBC-free plasma layer, the glycocalyx, the endothelium, the vascular wall, and smooth muscle tissue.

$$\frac{D_{NO}}{r}\frac{\partial}{\partial r}\left(r\frac{\partial C_{NO}}{\partial r}\right) - \lambda_b C_{NO} = 0 \tag{13}$$

where D_{NO} is the diffusion coefficient of NO in the RBC-rich core and λ_b is the reaction rate constant of NO scavenging by RBCs. For the value of membrane permeability determined in Ref. 58, λ_b is almost constant over the range of physiological Hct (57). We therefore set λ_b to the constant value shown in Table 1.

Plasma layer ($R - \delta \le r \le R$) and glycocalyx ($R \le r \le r_g$, where r_g is radial distance to the outer edge of the glycocalyx). The absence of RBCs in the plasma layer and glycocalyx allowed us to describe the transport of C_{NO} and P_{O_2} using the following steady-state diffusion equations:

$$\frac{D_{NO}}{r}\frac{\partial}{\partial r}\left(r\frac{\partial C_{NO}}{\partial r}\right) = 0 \tag{14}$$

$$\frac{\gamma D_{O_2}}{r}\frac{\partial}{\partial r}\left(r\frac{\partial P_{O_2}}{\partial r}\right) = 0 \tag{15}$$

where γ is the solubility of O_2 and D_{NO} and the diffusion coeffient of O_2 (D_{O_2}) in fluid phases (i.e., the plasma layer and RBC-rich core) are larger than their counterparts in the vascular wall and the other "solid" tissue phases (47).

Endothelium ($r_g \le r \le r_{en}$, where r_{en} is radial distance to the endothelium). The rate of O_2 consumption is assumed to be twice the rate of NO production (26, 51). C_{NO} and P_{O_2} satisfied a coupled system of the following steady-state reaction-diffusion equations:

$$\frac{D_{NO}}{r}\frac{\partial}{\partial r}\left(r\frac{\partial C_{NO}}{\partial r}\right) + R_e = 0 \tag{16}$$

$$\frac{\gamma D_{O_2}}{r}\frac{\partial}{\partial r}\left(r\frac{\partial P_{O_2}}{\partial r}\right) - 2R_e = 0 \tag{17}$$

Vascular wall ($r_{en} \le r \le r_w$, where r_w is radial distance to the vascular wall) and smooth muscle tissue ($r_w \le r \le r_m$, where r_m is radial distance to the smooth muscle tissue). Following Ref. 8, we assumed that NO undergoes a pseudo-first-order reaction and that O_2 consumption is inhibited by NO in accordance with Michaelis-Menten kinetics. The corresponding transport equations were as follows:

$$\frac{D_{NO}}{r}\frac{\partial}{\partial r}\left(r\frac{\partial C_{NO}}{\partial r}\right) - \lambda_t C_{NO} = 0 \tag{18}$$

$$\frac{\gamma D_{O_2}}{r}\frac{\partial}{\partial r}\left(r\frac{\partial P_{O_2}}{\partial r}\right) - R_m = 0, \tag{19}$$

with the peak O_2 consumption rate being lower in the vascular wall than in the muscle tissue, where, according to Ref. 8:

$$R_m = \frac{R_{O_2,max} P_{O_2}}{P_{O_2} + K_m^m} \tag{20}$$

$$K_m^m = 1 + \frac{C_{NO}}{27\ \text{nM}} \tag{21}$$

where $R_{O_2,max}$ is the maximal rate of O_2 consumption and λ_t is the rate of consumption of NO in tissue.

Boundary Conditions for NO and O_2 Transport

Since both C_{NO} and P_{O_2} are axisymmetric about the arteriole center $r = 0$, transport *Eqs. 13–21* are subject to the following boundary condition:

$$\frac{\partial C_{NO}}{\partial r}(r = 0) = 0 \text{ and } \frac{\partial P_{O_2}}{\partial r}(r = 0) = 0 \tag{22}$$

We assumed the absence of diffusive fluxes of C_{NO} and P_{O_2} across the outer boundary of the muscle tissue (at radial distance r_m from the vessel centerline) (26), such that:

$$\frac{\partial C_{NO}}{\partial r}(r = r_m) = 0 \text{ and } \frac{\partial P_{O_2}}{\partial r}(r = r_m) = 0 \tag{23}$$

Mass conservation across the interfaces between adjacent layers requires the following:

$$C_{NO}^- = C_{NO}^+,\ P_{O_2}^- = P_{O_2}^+,\ \left(D_{NO}\frac{\partial C_{NO}}{\partial r}\right)^- = \left(D_{NO}\frac{\partial C_{NO}}{\partial r}\right)^+,\ \text{and}\ \left(D_{O_2}\frac{\partial P_{O_2}}{\partial r}\right)^- = \left(D_{O_2}\frac{\partial P_{O_2}}{\partial r}\right)^+ \tag{24}$$

where the superscripts $-$ and $+$ indicate that the corresponding quantities were computed inside and outside of each interface, as shown in Fig. 3.

Numerical Implementation

Autoregulation. STEP 1. For a given value of Hct and ignoring the shear term φ in *Eq. 7*, we determined the constant C from experimental data for the myogenic response in vessels either with a denuded endothelium (16) or in the absence of flow (22, 46). The iterative procedure to determine C in *Eq. 7* was as follows:

A. Assume an initial value for C. We used an initial guess of $C = 0$, which corresponds to purely elastic, passive behavior.

B. Use *Eqs. 5–8* to calculate the deformation of the vessel for each of the incremental increases in pressure (ΔP) from 50 to 60 mmHg. We used $\Delta P = 0.001$ mmHg.

C. Compute the slope of the resulting (approximately) linear relationship between vessel radius and pressure.

D. Compare the calculated slope with that estimated from experimental data (in this study, data from Refs. 22 and 46). If the absolute difference between the calculated and experimentally observed slopes exceeds a prescribed tolerance (ε_1), increase C by Δ_1. We used $\varepsilon_1 = 10^{-3}$ and $\Delta_1 = 0.01$.

E. Repeat *steps 1B–1D* until the convergence criterion is met.

STEP 2. Once the value of C was computed, we accounted for shear stress. Specifically, we determined the constant α in *Eq. 8* by enforcing autoregulation, i.e., the condition that Q in *Eq. 1* remains constant with small changes in pressure. The iterative procedure to determine α in *Eq. 8* was as follows:

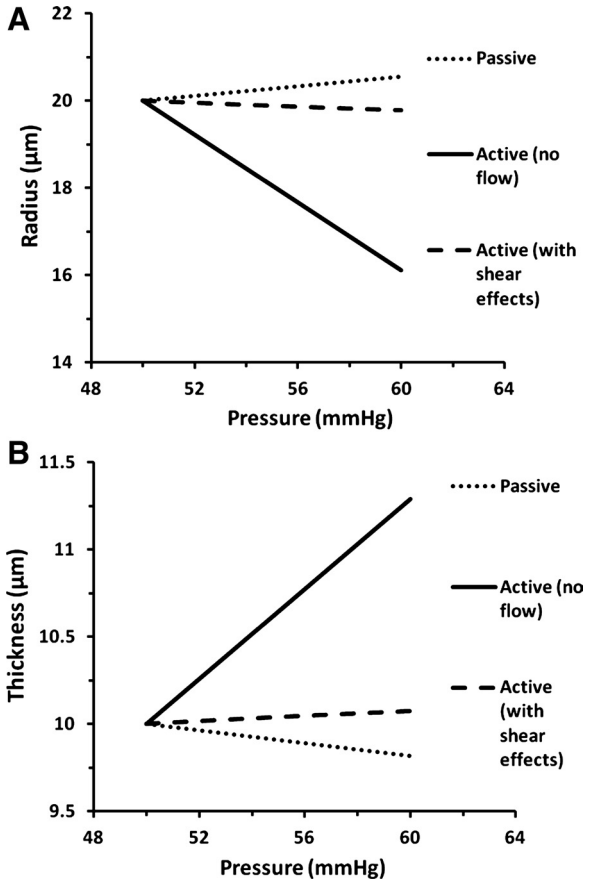

Fig. 4. *A* and *B*: variations of the vessel radius (*A*) and vessel thickness (*B*) with pressure for different mechanical responses.

A. Assume an initial value for α. We used a initial guess of $\alpha = 0$, which corresponds to a situation where WSS completely eliminates the myogenic response.

B. Use *Eqs. 5–9* to calculate the deformation of the vessel for each ΔP from 50 to 60 mmHg.

C. Compute Q values corresponding to each value of pressure using Eqs. *1–4*, *9*, and *10*. Plot the resulting Q versus P curve.

D. If the curve has a nonzero [up to a prescribed tolerance (ε_2)] slope, increase α by Δ_2. We used $\varepsilon_2 = 10^{-4}$ and $\Delta_2 = 0.0001$.

E. Repeat *steps 2B–2D* until the slope is zero (up to ε_2), i.e., until Q does not change with pressure.

Effect of varying Hct. STEP 3. We prescribed a functional dependence of P on H_d based on experimental data (31, 43). For parameters *C* and α computed in *steps 1* and *2*, we calculated the vessel's response to changes in H_d using the following algorithm:

A. Increase H_d by a small increment (Δ_H) = 0.001%.

B. Use *Eq. 10* to compute the new pressure for the new value of H_d.

C. Use *Eqs. 8* and *9* to calculate *J* and φ.

D. Use *Eqs. 4–7* to calculate the new vessel radius and thickness.

E. Use *Eqs. 1–3* to calculate the new Q.

F. Repeat *steps 3A–3E* to obtain a relationship between Q and H_d.

RESULTS

Changes of Vessel Diameter With Pressure

Figure 4*A* shows the variation of the arteriole inner radius with increasing intraluminal pressure. When the myogenic response is ignored (i.e., when only the passive response is considered), the vessel radius increased linearly with pressure. Conversely, including the myogenic response caused the arteriole radius to decrease. Ignoring the shear effects (and hence the endothelial NO production) enhanced the strength of the myogenic response modulated by WSS (22, 34). Setting $C = 8$ in *Eq. 7* yielded an active (no flow) response that matched well with the experimental data (27, 36, 45). Figure 4*B* shows the corresponding variation in vessel wall thickness. Passive and active mechanical responses to the small changes in pressure led to a linear relation between vessel radius and pressure. This finding was in agreement with experimental data (27, 36, 45), providing a justification for the assumption that the vessel behaves like a linear, elastic material for small variations in intraluminal pressure.

Figure 5 shows the dependence of flow rate on intraluminal pressure for several values of parameter α in *Eq. 8*. For $\alpha = 0.1434$, flow rate remained constant with small changes in pressure. This establishes autoregulation, which results from a balance between the relative strengths of the passive (elastic) and active (myogenic) responses in the blood vessel, with shear stress modulating the active response. In this autoregulatory regime, the vessel radius decreased marginally as pressure increased; small reductions in the vessel radius offset the increase in both the pressure gradient and, according to *Eq. 9*, pressure; this process resulted in the approximately constant flow rate.

Effect of Varying Hct

Figure 6, *A* and *B*, shows the dependence of both vessel radius and flow rate on systemic Hct, for pressure varying with Hct in the manner described in Refs. 31 and 43. When all parameters were selected to ensure autoregulation (corresponding to constant Hct), we found that flow rate significantly decreased with Hct. This finding was supported by the experimentally observed variation of CO with Hct (40) but was at odds with the experimental results reported in Refs. 31 and 43. The predicted reduction in flow rate can be attributed to the increase in blood viscosity with Hct while vessel dilation remained negligible. For larger values of *C* in *Eq. 7*, i.e., for a stronger myogenic response, the variation in flow rate with Hct resembled the behavior reported in Refs. 30 and 31. The

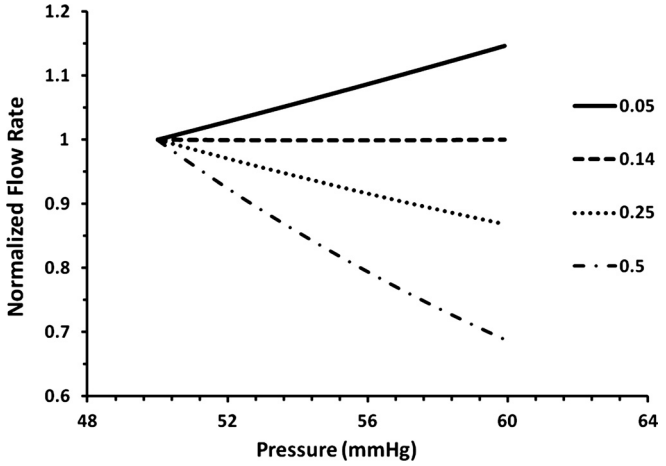

Fig. 5. Effect of varying parameter α on the dependence of flow rate with intraluminal pressure.

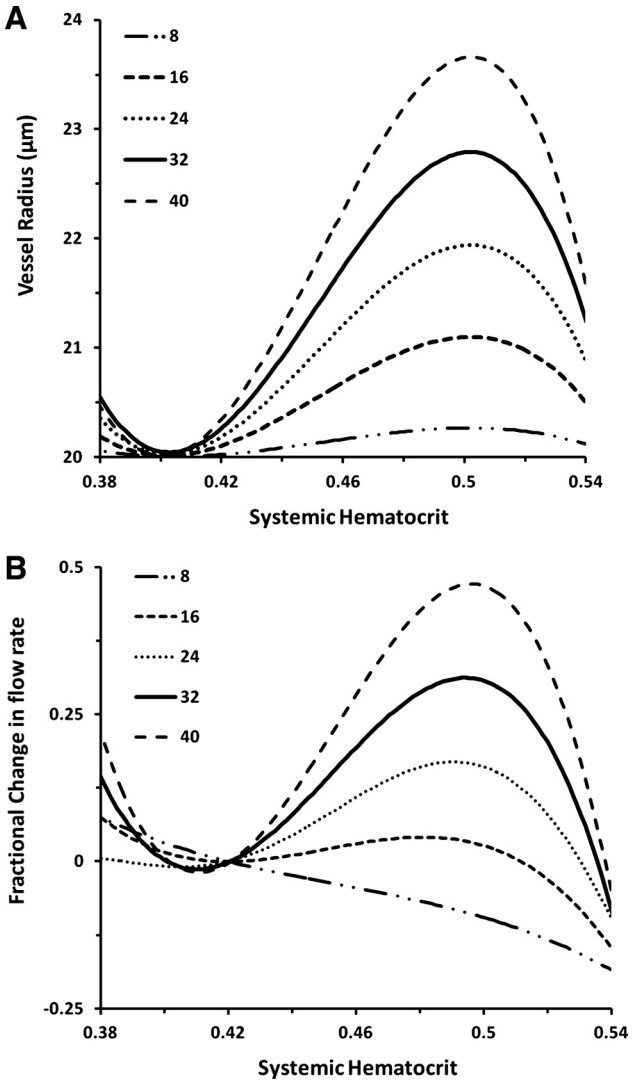

Fig. 6. *A* and *B*: variations of vessel radius (*A*) and flow rate (*B*) with Hct for different strengths of the myogenic response, governed by parameter *C* in *Eq. 7*.

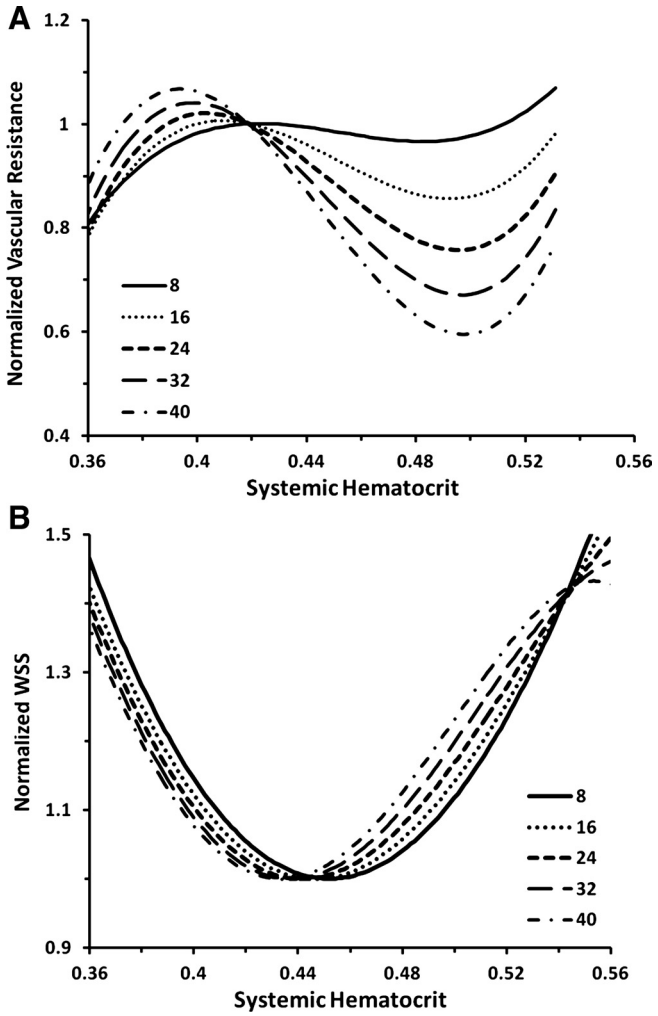

Fig. 7. *A* and *B*: variation of vascular resistance (VR; *A*) and wall shear stress (WSS; *B*) with Hct for different strengths of the myogenic response, governed by parameter *C* in *Eq. 7*.

stronger myogenic response offset autoregulatory control by changing the balance between the active and passive components of mechanical stress in the vessel walls. This suggests that during acute hemoconcentration and hemodilution, the ability to autoregulate was offset, similar to previously reported data for cerebral tissue exposed to hemodilution (35, 48).

Figure 7 shows the corresponding variation in vascular resistance (cardiac index divided by blood pressure; *A*) and WSS (*B*) with increasing Hct. For values of *C*, which predict variations in flow rate similar to those reported in Refs. 31 and 43, our model predicted a large reduction in vascular resistance and significant increases in WSS. This increases NO production and contributes to vasodilation. The predicted U-shaped curve for variations in vascular resistance was in agreement with calculations from experimental data (31, 43). Figure 8 shows experimental measurements of the dependence of vascular resistance on systemic Hct accompanied by the model predictions for $C = 32$ in *Eq. 7*.

Analysis of NO Concentration

Figure 9 shows the variation in NO concentration for different values of *L* in *Eq. 12*. This parameter controls the extent

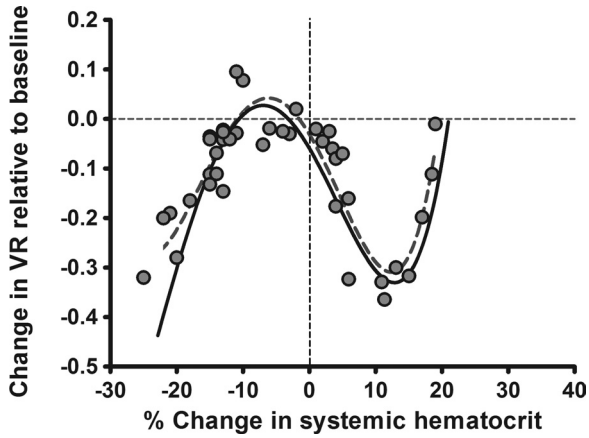

Fig. 8. Changes in VR with systemic Hct for $C = 32$ (solid line) and experimental data (31, 43) (dashed line).

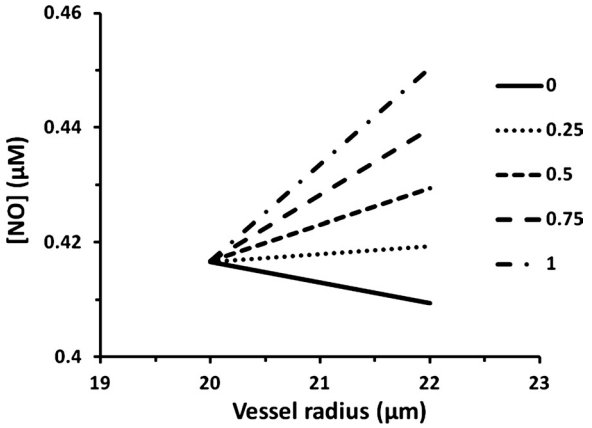

Fig. 9. Effect of parameter L in *Eq. 12* on variations of NO concentration with vessel radius.

of stretch-induced NO production. For $L = 0$, i.e., in the absence of stretch-induced NO production, NO concentration in the vessel wall fell marginally as radius increased. This decrease in NO concentration occurs because the increasing vessel radius increases the surface area across which NO diffuses into the bloodstream and is scavenged by RBCs. This causes NO bioavailability to fall, since the bloodstream scavenges NO at a high rate (26) and because NO has a higher diffusivity in blood than in tissue (17). In other words, the increasing radius enhances diffusion of NO produced by the endothelium into the bloodstream, where it is consumed by RBCs as opposed to its diffusion into surrounding tissue. The net effect is to reduce NO bioavailability in the vessel walls. Higher values of L, i.e., higher stretch-induced NO production, resulted in an increase of NO concentration with stretch (24, 59). Clearly, for NO to have a role as a vasodilator in this system, stretch-induced NO production must be significant. For this study, we used $L = 1$ as a representative value quantifying stretch-induced NO production.

Figure 10*A* shows the variation of average NO concentration with Hct for different values of C in *Eq. 7*. This parameter represents the strengths of active response, as shown in Fig. 6*A*; $C = 48$ resulted in a flow versus Hct relation that closely matched the results reported in Refs. 30, 31, and 40. Figure 10*A* shows the action of NO as a vasodilator in this system, with larger vessel radii corresponding to larger NO concentrations. To illustrate the importance of stretch-induced NO production on the vasodilatory role of NO, we plotted the variation of NO concentration with Hct for $C = 48$ and different values of L in *Eq. 12*. In the absence of stretch-induced NO production, NO bioavailability in the vessel wall actually dropped, reinforcing the idea that stretch-induced NO production is necessary for endothelial NO production to stimulate vasodilation in this system (Fig. 10*B*).

DISCUSSION

In the present report, we present a model for vessel mechanics that incorporates the elastic response and myogenic response modulated by shear effects for small changes in pressure and Hct. The comparison with experimental data (30, 31, 40) demonstrates that our model is capable of reproducing both active and passive responses of the arteriole over the range of pressure used in these experiments.

Our model assumes that the primary contributing factor to NO bioavailability in the vasculature is endothelial NO production stimulated by WSS and stretch (3), due to increased activation of endothelial NO synthase, and focuses on the effects of coupled of shear and myogenic responses on the autoregulation of blood flow. We found that physiologically relevant changes in microvascular regulation occurred when changes of vessel wall NO concentration were on the order of 0.1 μM. This finding is in general agreement with those of previous studies (9, 49, 53). The results shown in Figs. 6 and 9 demonstrate that our model accounts for the effect of this NO change (produced by the WSS-stimulated endothelium) on the myogenic response (22, 25, 34) and demonstrate how the NO concentration varies with WSS and vessel stretch.

Our results suggest that, in the range of pressure studied, a simple Hookean model for arteriolar mechanics is adequate to describe the passive and active responses of blood vessels, with the myogenic response modeled by *Eq. 7* as a function of tension in the vessel wall. Leveraging the thick cylinder theory, our model accounts for variations in wall thickness as well as

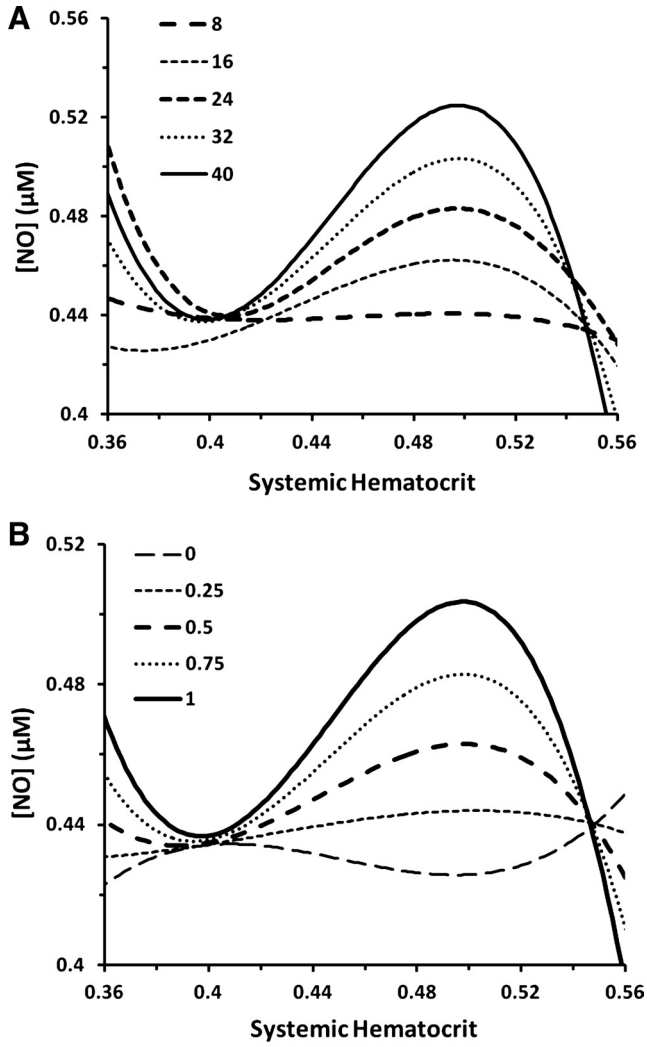

Fig. 10. *A*: variations of average NO concentration in the vessel wall for different values of parameter C in *Eq. 8* (and hence different strengths of the myogenic response) with $L = 1$ in *Eq. 12*. *B*: variations of NO concentration for different values of L in *Eq. 12* with $C = 32$.

changes in the vessel's inner radius. Using existing models of blood flow in arterioles (47, 51), the model couples the solid mechanics governing vessel deformation with the hemodynamics of arteriolar blood flow and relates changes in pressure to changes in flow rate. The two-layer fluid flow model used in this study accounts for the presence of a discrete plasma layer. An area of interest for future study is to understand how variations in plasma layer thickness and viscosity (56) influence this autoregulatory behavior. As shown in the APPENDIX, our results for variations of flow rate with Hct are relatively insensitive to the choice of rheological model, justifying the selection of the simple two-layer Newtonian model for blood flow used in this study.

Combined with the experimentally determined dependence of pressure on Hct (30, 31), our model sheds new light on how variations in Hct affect the flow rate in an arteriole (and hence CO). We found that this variation was heavily dependent on the balance between active (myogenic) and passive (elastic) responses (controlled by parameter *C* in *Eq. 7*). When these active and passive responses are balanced and achieve autoregulation (for constant Hct), the blood flow rate drops significantly as Hct increases. This behavior is due to the sharp increase in blood viscosity with increasing Hct (60); it is in agreement with an earlier study (40) that reported a linear decrease in CO with increasing Hct. We also demonstrated that the nonlinear behavior reported in Refs. 30, 31, and 43 is likely due to an offset in the balance between the active and passive responses, with the active (myogenic) response dominating (see Fig. 6). This sharper active response results in arteriolar dilatation (for reductions in pressure) and hence in increased flow rate. A previous study (35) has suggested a similar change in autoregulatory behavior in cerebral tissue for mild hemodilution.

The origin of this increased active response is a matter for future study. Possible explanations include this being a transient effect, since the mechanical response of blood vessels (4, 7, 15) and NO production (32, 33) vary with time; other aspects of the experimental procedure, such as the effect of anesthesia on muscle tone; or other stimuli, such as increased activation of the sympathetic nervous system, which has been associated with hemoconcentration (1). Understanding this unexpected response to acute hemoconcentration is important, as the underlying physiology may be crucial for predicting responses to blood transfusion, which are accompanied by acute fluctuations in Hct (19). Future study in this area (both experimental and theoretical) is needed to better understand the cardiac response due to RBC concentration/dilution and the underlying physiology.

We mathematically showed that stretch-induced NO production is crucial to the role of NO as a vasodilator (see Figs. 9 and 10). Without this stretch-induced mechanism, increasing vessel radius would cause NO levels in the vessel wall to drop, thereby eliminating the vasodilatory effect of NO. However, with stretch stimulating NO production by the endothelium, it is possible for NO levels to rise and be maintained at a higher level (relative to some baseline) as vessel radius is increased. This suggests the need for further study of stretch-induced NO production, especially to obtain more rigorous mathematical models of changes in NO production in response to changes in stretch. The importance of shear-induced NO production is qualitatively illustrated by the resulting NO bioavailability (Fig. 6*B*). The results shown in Figs. 6*A* and 10*A* demonstrated a relationship between NO bioavailability and vasodilation. They suggest that, in the range of physiological concentrations, there exists a simple constitutive relationship between NO concentrations in the vascular wall and the extent of modulation of myogenic responses.

The curves for NO concentration, flow rate, and vascular resistance led us to conclude that the physiological response to Hct variations occurs as a result of the combination of mechanical (i.e., fluid mechanics of blood flow and solid mechanics of vessel walls) and biochemical (i.e., metabolic factors and the vasodilatory effect of NO) effects. Each aspect influences the other since mechanical changes cause WSS variations, which, in turn, influence the biochemistry within the vessel wall (by increasing NO concentrations), which, in turn, influences the mechanical side of the problem by altering the strength of the Bayliss effect and hence changing vessel mechanics and blood flow. The result is a complex balance between various, often competing, mechanical and biochemical processes.

A hamster experimental study (41) in which the increase in Hct was induced by transfusing RBCs whose hemoglobin (Hb) was converted to metHb (and therefore did not scavenge NO) has elucidated the role of changes in NO bioavailability due to increased WSS. Increasing blood viscosity with metHb-converted RBCs significantly extended the range of the Hct increase before causing hypotension, since the increase of volume (concentration) of RBCs did not increase the rate of NO scavenging by Hb. In addition to these data, the paradoxical response of cardiac function to acute Hct variations was not observed in endothelial NO synthase knockout mice (30). This finding further strengthens the hypothesis that the physiological response to Hct variations discussed in this study is strongly influenced by endothelial NO production and its increase due to increased WSS.

These results serve to explain, in part, the perception that the transfusion of a single unit of blood could be of benefit, even though in general it is of little significance in terms of changes of O_2 carrying capacity. Furthermore, in restrictive transfusion practice, it could help decide whether to transfuse a single unit or two units. This is because transfusion of a unit of blood increases Hb (i.e., Hct) by 1 g/dl or 7%, which is the range of the maximal reduction of vascular resistance, whereas two units or 14% place the circulation in the range where vascular resistance increases above baseline (29). These simplified calculations were based on a Hct of 45% (Hb of 14 g/dl), which would not justify a blood transfusion and assumed an isovolemic change in Hct that does not occur in blood transfusions. Moreover, they were derived for our experimental model, where a scaling between experimental and human conditions has not been established.

In conclusion, our study establishes a mathematical model for the pressure response of arterioles by extending previous models (20, 45) and coupling this mechanical response with fluid flow within an arteriole that treats blood as a two-layer fluid with the presence of a distinct plasma layer. Applying this framework to model the regulatory response of arterioles with changes in Hct resulted in calculated variations in CO that matched experimental data, depending on model parameterization. We found that the reported anomalous variations in CO (30, 31, 43) are due to the combination of increased NO

production and bioavailability by the increased WSS and a shift in the balance between passive and active mechanical responses of the arteriole affecting the autoregulatory response. These results have considerable implications for the understanding physiological response to acute Hct variations associated with blood transfusion and blood losses, since they suggest a significant increase in perfusion after a modest increase in Hct associated with the infusion of a unit of packed RBCs that is independent of the change in O_2 carrying capacity.

Model Limitations and Scope for Future Work

First, our model neglects transient effects in both the viscoelastic response of arteriole walls (7) and NO production in response to changes in WSS (32, 33). These mechanical and biochemical phenomena suggest that modulation of the myogenic response by shear effects is time dependent.

Second, shear-induced NO production has steady and transient components; acute changes in WSS induce gradual changes in NO production, until a new steady state is reached (32, 33). This effect can be analyzed by including a time-dependent decay function for the transient element of shear-induced NO production in *Eq. 12*, which relates NO production with WSS. Incorporation of these transient effects will establish the timescales needed for the system to reach the steady state examined in this study.

Third, the arteriole was modeled as an isotropic material with a constant elastic modulus. However, an arteriole's elastic modulus in the longitudinal direction is higher than its counterpart in the circumferential direction (15). Future studies will account for this anisotropy. Furthermore, an arteriole's elastic modulus is not constant but varies with radius. For small deformations, this is not a significant problem; however, for larger deformations (and variations in pressure), this variation of elastic modulus with radius might become important.

The thick cylinder theory used in our analysis can be used in followup studies to better understand the mechanical behavior of the vessel wall, such as the effects of Poisson's ratio of the vascular wall on vessel deformation (44).

Fourth, our study deals with a single arteriole rather than a network of blood vessels. Future studies of autoregulation in networks of blood vessels would provide a more realistic picture of autoregulation in a whole organ (14, 39). Completion of the description of the autoregulatory behavior of an entire network requires accounting for long-range "conducted" responses, where signals from individual blood vessels are conducted to neighboring vessels, ultimately coupling the responses of most vessels. Thus, dilation/constriction of upstream large vessels results in corresponding dilation/constriction of vessels downstream. This effect can be accounted for by introducing an additional component into the active response component of our model (*Eq. 7*), so that active stresses are also a function of signals conducted from other points in the network.

Fifth, future refinements of our model will also account for the action of vasoactive substances other than NO, e.g., the release of endothelin (a powerful vasoconstrictor that counteracts the dilatory effects of NO) from the endothelium and the release of prostacyclin (another potent vasodilator).

Finally, to make these studies relevant to conditions of transfusion medicine, it will be important to repeat the analysis and experimental program to deal with changes of Hct in animals that are at lower Hct baseline, as would be the case in medical practice.

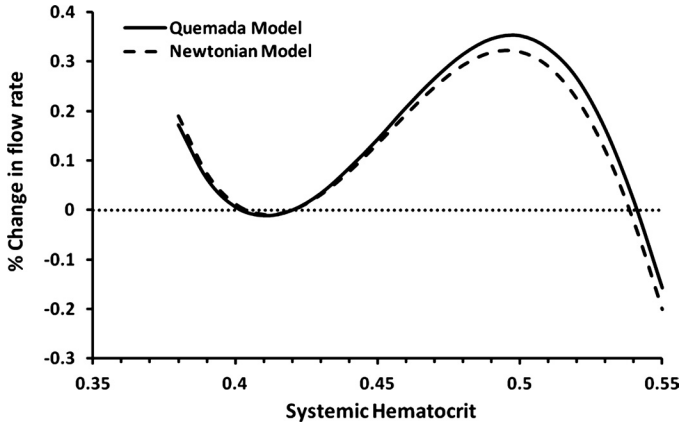

Fig. 11. Variations of flow rate with systemic Hct using both the Newtonian model for blood viscosity (*Eq. 2* in Ref. 51) and the Quemada shear thinning model (52) for $C = 32$ in *Eq. 7*.

APPENDIX: USING ALTERNATIVE RHEOLOGICAL MODELS FOR BLOOD

Our treatment of blood as a Newtonian fluid is an approximation, as blood is typically modeled as a non-Newtonian fluid (52) that exhibits shear-thinning behavior. Modeling blood as a non-Newtonian fluid typically involves expressing blood viscosity as a function of Hct as well as shear rate. An example of the rheological models used to describe blood as a non-Newtonian fluid is the Quemada model, which was used to explore the behavior of plasma expanders (52). Using the Quemada model instead of the Newtonian model to describe the rheology of the RBC-rich core in an arteriole, we followed the procedure outlined in Ref. 52 to calculate velocity profiles in the arteriole and to examine how flow rate varies with Hct. This enabled us to verify that our results are not simply the consequence of an incomplete rheological model for blood. We found that our results were relatively insensitive to the rheological model chosen and that our results (and conclusions) should hold even when blood is treated as a shear-thinning, non-Newtonian fluid. To demonstrate this, Fig. 11 shows the predicted variation of flow rate with systemic Hct using both the Newtonian and Quemada rheological models. The difference in predicted values between the two models was small, and the same general relationship between flow rate and systemic hematocrit was preserved.

GRANTS

This work was supported in part by National Heart, Lung, and Blood Institute (NHLBI) Bioengineering Research Partnership Grant R24-HL-064395 (to M. Intaglietta), by NHLBI Grants R01-HL-062354 (to M. Intaglietta) and R01-HL-076182 (to P. Cabrales), and by United States Army Medical Research Acquisition Activity Award W81XWH1120012 (to A. G. Tsai).

DISCLOSURES

No conflicts of interest, financial or otherwise, are declared by the author(s).

AUTHOR CONTRIBUTIONS

Author contributions: K.S., P.C., M.I., and D.M.T. conception and design of research; K.S., B.Y.S.V., A.G.T., and P.C. analyzed data; K.S., B.Y.S.V., A.G.T., and P.C. interpreted results of experiments; K.S., A.G.T., and P.C. prepared figures; K.S. drafted manuscript; K.S., M.I., and D.M.T. edited and revised manuscript; K.S., M.I., and D.M.T. approved final version of manuscript; B.Y.S.V., A.G.T., and P.C. performed experiments.

REFERENCES

1. **Allen MT, Patterson SM.** Hemoconcentration and stress: a review of physiological mechanisms and relevance for cardiovascular disease risk. *Biol Psychol* 41: 1–27, 1995.
2. **Arnold WP, Mittal CK, Katsuki S, Murad F.** Nitric oxide activates guanylate cyclase and increases guanosine 3′:5′-cyclic monophosphate levels in various tissue preparations. *Proc Natl Acad Sci USA* 74: 3203–3207, 1977.
3. **Balligand JL, Feron O, Dessy C.** eNOS activation by physical forces: from short-term regulation of contraction to chronic remodeling of cardiovascular tissues. *Physiol Rev* 89: 481–534, 2009.
4. **Bergel DH.** The static elastic properties of the arterial wall. *J Physiol* 156: 445–457, 1961.
5. **Birchard GF.** Optimal hematocrit: theory, regulation and implications. *Am Zool* 37: 65–72, 1997.
6. **Borgström P, Grande PO, Mellander S.** A mathematical description of the myogenic response in the microcirculation. *Acta Physiol Scand* 116: 363–376, 1982.
7. **Branigan T, Bolster D, Salazar Vázquez BY, Intaglietta M, Tartakovsky DM.** Mean arterial pressure nonlinearity in an elastic circulatory system subjected to different hematocrits. *Biomech Model Mechanobiol* 10: 591–598, 2011.
8. **Buerk DG.** Can we model nitric oxide biotransport? A survey of mathematical models for a simple diatomic molecule with surprisingly complex biological activity. *Ann Rev Biomed Eng* 3: 109–143, 2001.
9. **Carter TD, Bettache N, Ogden D.** Potency and kinetics of nitric oxide-mediated vascular smooth muscle relaxation determined with flash photolysis of ruthenium nitrosyl chlorides. *Br J Pharmacol* 122: 971–973, 1997.
10. **Chatpun S, Cabrales P.** Cardiac mechanoenergetic cost of elevated plasma viscosity after moderate hemodilution. *Biorheology* 47: 225–237, 2010.
11. **Cornelissen AJ, Dankelman J, VanBavel E, Spaan JA.** Balance between myogenic, flow-dependent, and metabolic flow control in coronary arterial tree: a model study. *Am J Physiol Heart Circ Physiol* 282: H2224–H2237, 2002.
12. **Davis MJ, Hill MA.** Signaling mechanisms underlying the vascular myogenic response. *Physiol Rev* 79: 387–423, 1999.
13. **Devereux RB, Case DB, Alderman MH, Pickering TG, Chien S, Laragh JH.** Possible role of increased blood viscosity in the hemodynamics of systemic hypertension. *Am J Cardiol* 85: 1265–1268, 2000.
14. **Diep HK, Vigmond EJ, Segal SS, Welsh DG.** Defining electrical communication in skeletal muscle resistance arteries: a computational approach. *J Physiol* 568: 267–281, 2005.
15. **Dobrin PB.** Mechanical properties of arteries. *Physiol Rev* 58: 397–460, 1978.
16. **Falcone JC, Davis MJ, Meininger GA.** Endothelial independence of myogenic response in isolated skeletal muscle arterioles. *Am J Physiol Heart Circ Physiol* 260: H130–H135, 1991.
17. **Fischkoff S, Vanderkooi JM.** Oxygen diffusion in biological and artificial membranes determined by the fluorochrome pyrene. *J Gen Physiol* 65: 663–676, 1975.
18. **Gertz KH, Mangos JA, Braun G, Pagel HD.** Pressure in the glomerular capillaries of the rat kidney and its relation to arterial blood pressure. *Pflügers Arch* 288: 369–374, 1966.
19. **Harder L, Boshkov L.** The optimal hematocrit. *Crit Care Clin* 26: 335–354, 2010.
20. **Johnson PC.** Autoregulation of blood flow. *Circ Res* 59: 483–495, 1986.
21. **Johnson PC.** Autoregulatory responses of cat mesenteric arterioles measured in vivo. *Circ Res* 22: 199–212, 1968.
22. **Juncos LA, Carretero OA, Ito S.** Flow modulates myogenic responses in isolated microperfused rabbit afferent arterioles via endothelium-derived nitric oxide. *J Clin Invest* 95: 2741–2748, 1995.
23. **Kleinstreuer N, David T, Plank MJ, Endre Z.** Dynamic myogenic autoregulation in the rat kidney: a whole-organ model. *Am J Physiol Renal Physiol* 294: F1453–F1464, 2008.
24. **Kuebler WM, Uhlig U, Goldmann T, Schael G, Kerem A, Exner K, Martin C, Vollmer E, Uhlig S.** Stretch activates nitric oxide production in pulmonary vascular endothelial cells in situ. *Am J Respir Crit Care Med* 168: 1391–1398, 2003.
25. **Lai EY, Onozato ML, Solis G, Aslam S, Welch WJ, Wilcox CS.** Myogenic responses of mouse isolated perfused renal afferent arterioles: effects of salt intake and reduced renal mass. *Hypertension* 55: 983–989, 2010.
26. **Lamkin-Kennard KA, Buerk DG, Jaron D.** Interactions between NO and O_2 in the microcirculation: a mathematical analysis. *Microvasc Res* 68: 38–50, 2004.
27. **Loutzenhiser R, Bidani A, Chilton L.** Renal myogenic response: kinetic attributes and physiological role. *Circ Res* 90: 1316–1324, 2002.
28. **Lowe GD, Lee AJ, Rumley A, Price JF, Fowkes FG.** Blood viscosity and risk of cardiovascular events: the Edinburgh Artery Study. *Br J Haematol* 96: 168–173, 1997.
29. **Ma M, Eckert K, Ralley F, Chin-Yee I.** A retrospective study evaluating single-unit red blood cell transfusions in reducing allogeneic blood exposure. *Transfus Med* 15: 307–312, 2005.
30. **Martini J, Carpentier B, Chávez Negrete A, Frangos JA, Intaglietta M.** Paradoxical hypotension following increased hematocrit and blood viscosity. *Am J Physiol Heart Circ Physiol* 289: H2136–H2143, 2005.
31. **Martini J, Tsai AG, Cabrales P, Johnson PC, Intaglietta M.** Increased cardiac output and microvascular blood flow during mild hemoconcentration in hamster window model. *Am J Physiol Heart Circ Physiol* 291: H310–H317, 2006.
32. **Mashour GA, Boock RJ.** Effects of shear stress on nitric oxide levels of human cerebral endothelial cells cultured in an artificial capillary system. *Brain Res* 842: 233–238, 1999.
33. **McAllister TN, Frangos JA.** Steady and transient fluid shear stress stimulate NO release in osteoblasts through distinct biochemical pathways. *J Bone Miner Res* 14: 930–936, 1999.
34. **Nurkiewicz TR, Boegehold MA.** Limitation of arteriolar myogenic activity by local nitric oxide: segment-specific effect of dietary salt. *Am J Physiol Heart Circ Physiol* 277: H1946–H1955, 1999.
35. **Ogawa Y, Iwasaki K, Aoki K, Shibata S, Kato J, Ogawa S.** Central hypervolemia with hemodilution impairs dynamic cerebral autoregulation. *Anesth Analg* 105: 1389–1396, 2007.
36. **Park KW, Dai HB, Lowenstein E, Sellke FW.** Steady-state myogenic response of rat coronary microvessels is preserved by isoflurane but not by halothane. *Anesth Analg* 82: 969–974, 1996.
37. **Patel DJ, Fry DL.** Longitudinal tethering of arteries in dogs. *Circ Res* 19: 1011–1021, 1966.
38. **Plunkett CW, Overbeck HW.** Increased arteriolar wall-to-lumen ratio in a normotensive vascular bed in coarctation hypertension. *Am J Physiol Heart Circ Physiol* 249: H859–H866, 1985.
39. **Pries AR, Secomb TW, Gaehtgens P.** Structural autoregulation of terminal vascular beds: vascular adaptation and development of hypertension. *Hypertension* 33: 153–161, 1999.
40. **Richardson TQ, Guyton AC.** Effects of polycythemia and anemia on cardiac output and other circulatory factors. *Am J Physiol* 197: 1167–1170, 1959.
41. **Salazar Vázquez BY, Cabrales P, Tsai AG, Johnson PC, Intaglietta M.** Lowering of blood pressure by increasing hematocrit with non nitric oxide scavenging red blood cells. *Am J Respir Cell Mol Biol* 38: 135–142, 2008.
42. **Salazar Vázquez BY, Martini J, Chávez-Negrete A, Cabrales P, Tsai AG, Intaglietta M.** Microvascular benefits of increasing plasma viscosity and maintaining blood viscosity: Counterintuitive experimental findings. *Biorheology* 46: 167–179, 2009.
43. **Salazar Vázquez BY, Martini J, Tsai AG, Johnson PC, Cabrales P, Intaglietta M.** The variability of blood pressure due to small changes of hematocrit. *Am J Physiol Heart Circ Physiol* 299: H863–H867, 2010.
44. **Sarma PA, Pidaparti RM, Meiss RA.** Anisotropic properties of tracheal smooth muscle tissue. *J Biomed Mater Res A* 65: 1–8, 2003.
45. **Schubert R, Mulvany MJ.** The myogenic response: established facts and attractive hypotheses. *Clin Sci (Lond)* 96: 313–326, 1999.
46. **Secomb TW.** Theoretical models for regulation of blood flow. *Microcirculation* 15: 765–775, 2008.
47. **Sharan M, Popel AS.** A two-phase model for flow of blood in narrow tubes with increased effective viscosity near the wall. *Biorheology* 38: 415–428, 2001.
48. **Shoemaker JK.** Hemodilution impairs cerebral autoregulation, demonstrating the complexity of integrative physiology. *Anesth Analg* 105: 1179–1181, 2007.
49. **Simonsen U, Wadsworth RM, Buus NH, Mulvany MJ.** In vitro simultaneous measurements of relaxation and nitric oxide concentration in rat superior mesenteric artery. *J Physiol* 516: 271–282, 1999.
50. **Skalak TC, Price RJ.** The role of mechanical stresses in microvascular remodeling. *Microcirculation* 3: 143–165, 1996.

51. **Sriram K, Salazar Vázquez BY, Yalcin O, Johnson PC, Intaglietta M, Tartakovsky DM.** The effect of small changes in hematocrit on nitric oxide transport in arterioles. *Antioxid Redox Signal* 14: 175–185, 2011.
52. **Sriram K, Tsai AG, Cabrales P, Meng F, Acharya SA, Tartakovsky DM, Intaglietta M.** PEG-albumin supraplasma expansion is due to increased vessel wall shear stress induced by blood viscosity shear thinning. *Am J Physiol Heart Circ Physiol* 302: H2489–H2497, 2012.
53. **Tare M, Parkington HC, Coleman HA, Neild TO, Dusting GJ.** Hyperpolarization and relaxation of arterial smooth muscle caused by nitric oxide derived from the endothelium. *Nature* 346: 69–71, 1990.
54. **Taylor LA, Gerrard JH.** Pressure-radius relationships for elastic tubes and their application to arteries: part 1–theoretical relationships. *Med Biol Eng Comput* 15: 11–17, 1977.
55. **Timoshenko S.** *Theory of Elasticity*. Columbus, OH: McGraw-Hill, 1934.
56. **Tsai AG, Acero C, Nance PR, Cabrales P, Frangos JA, Buerk DG, Intaglietta M.** Elevated plasma viscosity in extreme hemodilution increases perivascular nitric oxide concentration and microvascular perfusion. *Am J Physiol Heart Circ Physiol* 288: H1730–H1739, 2005.
57. **Tsoukias NM, Popel AS.** Erythrocyte consumption of nitric oxide in presence and absence of plasma-based hemoglobin. *Am J Physiol Heart Circ Physiol* 282: H2265–H2277, 2002.
58. **Vaughn MW, Huang KT, Kuo L, Liao JC.** Erythrocyte consumption of nitric oxide: competition experiment and model analysis. *Nitric Oxide* 5: 18–31, 2001.
59. **Wei B, Chen Z, Zhang X, Feldman M, Dong XZ, Doran R, Zhao BL, Yin WX, Kotlikoff MI, Ji G.** Nitric oxide mediates stretch-induced Ca^{2+} release via activation of phosphatidylinositol 3-kinase-Akt pathway in smooth muscle. *PLos One* 3: e2526, 2008.
60. **Wells RE Jr, Merrill EW.** Influence of flow properties of blood upon viscosity-hematocrit relationships. *J Clin Invest* 41: 1591–1598, 1962.
61. **Whirlow DK, Rouleau WT.** Periodic flow of a viscous liquid in a thick-walled elastic tube. *Bull Math Biophys* 27: 355–370, 1965.